

VISUALISATION STRATEGIES FOR COMPUTATIONAL THERMO FLUID DYNAMICS

Mallinson, G.D.* and Norris, S.E.

*Author for correspondence

Department of Mechanical Engineering,

The University of Auckland,

Auckland, 1142,

New Zealand,

E-mail: g.mallinson@auckland.ac.nz

ABSTRACT

This paper considers the challenges of visualising data that describe thermo fluid dynamic processes. The importance of being able to construct visualisation artefacts that accurately represent the properties of relevant transport vectors is discussed and appropriate methods based on vector and scalar potentials are described. Attention then turns to heatlines which are becoming increasingly popular for visualising heat transfer process but suffer from ambiguities that arise from the choice of conditions for reference enthalpy. Fortunately, although the assumed reference conditions influence the heatline patterns within the flow, the overall heat transfer analysis provided by the lines may not be adversely affected. The possibility of extending the heatline approach to entropy lines is then considered for two and three dimensional heat transfer fields. The entropy transport vector is not divergence free and a new method that involves a combination of scalar and vector potentials is proposed to correctly construct the lines of the entropy transport vector.

INTRODUCTION

Computational thermo fluid dynamics (CTFD) is capable of predicting complex 3D and 4D steady or unsteady scalar and vector data fields that represent the underlying physical processes. The challenge for several decades has been to find appropriate methods to visualise and interpret those fields.

As early as the 1960s, the Los Alamos group's visualisations of waves and drops impacting with a liquid surface [1,2] demonstrated the efficacy of what is now recognised as computational fluid dynamics (CFD) visualisation. Fromm [3] produced streamlines and streak lines past an obstacle by tracking contours of a stream function using linear interpolation. In those days computer "plots" were output to magnetic tape and then to a microfilm recorder. Fromm made the comment that "the computer time consumed in obtaining the output is roughly 10% of the overall time of an

average calculation." With increased flow complexity that fraction is now considerably greater and visualization becomes the dominant part of a thermo fluid dynamic study.

Ideally a visualisation strategy should have the ability to rapidly display the essential characteristics of a thermo fluid dynamic process. The artefact created in the visualisations should be accurate and not lead to false interpretation. Quantitative data produced by the visualisations should correctly relate to the underlying physical laws on which the modelling relies.

An added motivation for the generation of simple methods for visualising complex CTFD data is the widespread development of coupled computer aided design and modelling packages. Concerns arising from relatively naïve use of CTFD in design leads to consideration of how visualisation and post processing might be improved so that CTFD is used correctly and the right interpretations are made.

The perspective taken here is that "whole field" methods that can be applied in one step are preferable to local exploratory tools that take many iterations to reveal the characteristics of a field. For example 2D steady incompressible flow can be represented by a single contour map of a stream function which also provides quantitative data about volume flow rates. Unfortunately, if an additional spatial dimension is involved, the flow becomes unsteady or is compressible, compact whole field visualisations become virtually impossible.

As will be discussed in the next Section, currently available visualisation tools apply to scalar or vector fields and have been developed generally in the context of CFD. The representation of a process involving thermodynamics or heat transfer requires the creation of relevant scalar or vector fields that can be processed by CFD visualisation tools. For example, the heat function introduced by Kimura and Bejan [4] relates to 2D steady state convection in a manner similar to the way that a stream function does for fluid motion. This concept is expanded

here by considering the role of generalised transport vectors, of which the heat flux vector that underpins heatlines is an example, have in providing new visualisation strategies. The simple example of natural convection in a box is used to demonstrate that despite the fact that visualisation tools have been available for several decades, there is much to learn about how accurate and meaningful visualisation artefacts can be constructed.

The discussion is guided by prior experience with creating algorithms to construct vector lines, e.g. streamlines and vortex lines, that accurately represent the divergence of the vector. These aspects are summarised in the following section, and lead to the premise that scalar and vector potentials should be used as part of the visualisation strategy.

NOMENCLATURE

ds	$[m^2]$	Element of area
dv	$[m^3]$	Element of volume
e	$[W/m^2]$	Specific energy
\mathbf{e}	$[-]$	Generalised transport vector
f	$[m^2/s]$	Dual stream function
g	$[m^2/s]$	Dual Stream function
\mathbf{g}	$[m/s^2]$	Gravitational acceleration vector
H	$[W/m]$	Heat function
k	$[W/mK]$	Thermal conductivity
$\dot{\mathbf{q}}$	$[W/m^2]$	Heat flux vector
\dot{q}'''	$[W/m^3]$	Volumetric heat generation density
p	$[N/m^2]$	Pressure
r	$[m]$	Position vector
Pr	$[-]$	Prandtl number
Ra	$[-]$	Rayleigh number
s	$[J/kgK]$	Specific entropy
\mathbf{s}	$[W/m^2K]$	Entropy transport vector
t	$[s]$	Time
T	$[K]$	Temperature
\mathbf{u}	$[m/s]$	Velocity vector = $u\hat{\mathbf{i}} + v\hat{\mathbf{j}} + w\hat{\mathbf{k}}$
V	$[m^3]$	Volume
x	$[m]$	Cartesian axis direction
y	$[m]$	Cartesian axis direction
z	$[m]$	Cartesian axis direction
Special characters		
ζ	$[/s]$	Vorticity
ζ	$[/s]$	Vorticity scalar or vector component
Ψ	$[m^2/s]$	Vector potential for velocity
ψ	$[m^2/s]$	Stream function or component of vector potential
Ψ_e	$[kg/ms]$	Vector potential for energy transport vector
Φ	$[/s^2]$	Viscous dissipation function
ε	$[-]$	Non dimensional temperature difference, Eq (52).
ρ	$[kg/m^3]$	Density
θ	$[-]$	Non dimensional temperature
σ	$[kg/ms^2]$	Deviatoric stress tensor
μ	$[Nm/s^2]$	Dynamic viscosity
Subscripts		
ref		Reference
S		Surface
T		Temperature or thermal energy
x		Cartesian Coordinate
y		Cartesian Coordinate
z		Cartesian Coordinate

VISUALISATION BACKGROUND

Basic Visualisation Methods

With the advent of 3D vector refresh displays in the mid 1960s, interactive visualisation of 3D computational models became a reality and by the early 1970s basic tools for CFD visualisation were established. These included:

- 2D vector maps on plane or curved surfaces
- 2D contour maps using lines and filled shading
- 2D and 3D vector tangent lines used to represent particle paths, streamlines or vortex lines.

For example, particle tracks or streamlines were used [5-7] to visualise 3D solutions for natural convection in enclosures and an animated film was listed in [8] as being available for circulation to interested researchers (involving several months turn-around using cost effective postal options of the day). Initial uptake of these visualisation technologies was slow because computational resources were limited and most CFD solutions were 2D and presented no real visualisation challenges.

This is, of course, not the situation today. It is possible to generate CFD simulations of very complicated flows involving data sets having 10^{10} (and even this is probably an underestimate) degrees of freedom and there is a real challenge to unravel these data sets to properly understand them and the underlying thermo fluid dynamics. The requirement to visualise 3D steady or unsteady fields is now common place. However visualisation strategies have not kept up with the pace of development of the numerical solutions. The basic set of visualisation techniques has been augmented to include:

- iso-surface extraction using surface methods or volume visualisation
- flow feature detection.

Despite the considerable advances in flow detection algorithms, the majority of thermodynamics research publications use the first 4 of these visualisation methods.

The Relevance of Scalar and Vector Potentials

Vector potentials or dual scalar stream functions can be used to represent 3D vector fields and early CTFD solutions ([6], [8]) of 3D natural convection cavity flows used vector potential – vorticity methods.

A velocity vector \mathbf{u} can be related to a vector potential Ψ via:

$$\mathbf{u} = \nabla \times \Psi \quad (1)$$

The vector potential is usually chosen so that it is solenoidal, i.e.:

$$\nabla \cdot \Psi = 0 \quad (2)$$

There is, unfortunately, no direct relationship between a vector potential and the lines or stream surfaces of the velocity field that it represents. In practice issues associated with the prescription of boundary conditions for the vector potential and its lack of utility for visualisation meant that the vector potential – vorticity method has been almost completely bypassed in favour of primitive variable, (velocity – pressure) CTFD methods.

Streamlines or particle paths first started to appear in the literature in the early 1970s when they were used to display the flow in 3D natural convection and forced flows in enclosures, [6] and [7]. It was soon realised that the integration method used to track the paths had to be at least 4th order Runge Kutta and more significantly the velocity component interpolations had to satisfy mass conservation exactly, ([8]) so as not to introduce false sources that manifest as spiralling lines. Unfortunately even today, this is a too common reality. The majority of vector line methods used in commercial software exhibit such artefacts arising from well documented (e.g. [9]) inaccuracies in either path integration or field interpolation.

Although it is possible to generate volume conserving velocity interpolations directly these may require information from the CFD solver which is not always possible. However, volume conserving interpolation is readily achieved when a vector potential is available as part of the solution process. The velocity at a given point can be found by taking the curl of an interpolated vector potential [8]. Applying this idea in a visualisation strategy means finding the vector potential for a given velocity field [10]. As will be demonstrated in this paper, finding scalar or vector potentials for a given velocity field can be an effective part of a visualisation strategy.

Dual Stream Functions for Whole Field Visualisation

An alternative representation uses two potentials referred to as dual scalar stream functions and the velocity vector is represented by:

$$\mathbf{u} = \nabla f \times \nabla g \quad (3)$$

Iso-surfaces of the functions f and g are stream surfaces of the flow. Intersections between the two families of iso-surfaces are streamlines. However, as discussed in [10], at least one of the functions has very complicated iso-surfaces and the visualisation strategy has not been applied in general.

For flows where there is no recirculation or spiralling, dual stream functions can be applied for both visualisation and the solution process. There is a large body of research describing the application of dual stream functions to duct flows (e.g. [11], [12], [13]).

Beale [14] derived anisotropic diffusion equations relating dual stream functions to the velocity field which he solved numerically. His results presented in [14] and [15] show promising definition of the structure of flows around an obstacle and in a free vortex. However, the stream lines for the free vortex do not exhibit spirals that should arise from axial flow and this discrepancy, for which an explanation has not yet been found, remains a topic for future research.

If dual stream functions cannot easily be used for whole field visualisation, then they might be useful for constructing vector lines and surfaces within cells, where the flow can assumed to be simple and non vortical. This approach has been used to successfully trace stream lines for steady flows for structured [16] and unstructured grids [17,18].

Heatlines

Kimur and Bejan [4] were the first to use a heat function to visualise convection. Their demonstration for 2D natural convection in a square cavity showed that iso-lines of the heat function, which are the tangent lines of the heat flux vector field, behaved in an intuitively satisfying manner. The technique relied on the construction of a heat function which behaved for the heat flux vector in the same way that a stream function does for a 2D velocity field. The interval between a pair of heatlines is proportional to the heat flow rate between them. Heatlines can be used to understand the total heat flow balance for a flow in the same way that iso-lines of a stream function relate to volume flow rates. Following the initial development of the heat function concepts and application to several examples [19] the heatlines are sometimes referred to as Bejan's heatlines, (e.g. [20]).

Subsequent to this initial development the heatlines concept has been extended to mass lines and applications have included porous and anisotropic media, (e.g. [21-23]). and refer to [5] for a good list of heatline references). The use of the heat function and heatlines has started to permeate into the heat transfer literature with authors illustrating their works with heat function maps alongside stream function and temperature maps, (e.g refer to [20,24,25] for comprehensive lists of related publications).

Despite the popularity of heatlines, there is an issue that should be reconsidered. The heat flux vector as defined in [4], has two terms, one representing heat conduction and the other convection. The magnitude of the convection term depends on the local specific enthalpy, or, $c_p(T-T_{ref})$. The assumed reference condition for enthalpy or temperature determines the magnitude of the convection part of the heat flux vector and hence its direction. In practice this means that the direction of a heatline depends on the assumed reference condition. In [4], dimensionless variables were used and these led naturally to the use of the coldest temperature in the cavity as the reference temperature. This convention has persisted and most users of heatlines make this assumption without explicit statement.

The universal adoption of a common convention has masked the fact that the form of the heat function depends on an assumed reference condition for enthalpy and hence resulting visualizations are dependent on a parameter that does not influence any other aspect of the mathematical analysis or the computational model. This concern is heightened by recent extensions of the heatline approach to transient and 3D heat transfer problems [26-28] wherein the visualizations are becoming increasingly complicated. For example, in [27] stagnation points in the heat flux field have been reported for unsteady flows. When the chosen reference temperature is the coldest temperature in the domain, it is possible for the heat flux to stagnate locally within the domain. However these stagnation points may be artefacts arising from the reference condition choice.

One of the motivations of this discussion is to explore the effect of the reference condition. As a by-product of the investigation, the assumption that the temperature field is not a good indicator of the convection process [4], is challenged.

The Heat Function as Part of a More General Visualisation Strategy

The initial development of the heatline visualisation process (e.g. [4,19,29]) was presented in terms of the heat function rather than the related heat flux vector field. The heat function can be found only for two dimensional fields that have zero divergence which limits its application to steady convective flows without heat generation.

Only recently [10,26-28] has the construction of heatlines directly from the heat flux vector field been applied, the motivation being to extend the visualisation to 3D or unsteady flows. The heatline visualisation method therefore falls into a more general category of vector field visualisation with all the inherent difficulties of ensuring that the structure of the vector field and its properties such as zero divergence, if applicable, are correctly displayed by the visualizations [10].

Transport Vectors

The heat flux vector that underpins heatline visualisations is an example of the more general concept of transport vectors [10,26,30] that exist for quantities such as momentum, total energy, mechanical energy, thermal energy, mass and entropy. The tangent lines of these fields are transport lines of which heatlines are an example.

This paper describes the heatlines and the heat function as being embedded in the more general context of the transport vectors. All of these are subject to the reference temperature issue.

CONCEPTS

This section will present the concepts that underpin transport vectors and visualisation strategies that involve vector and scalar potentials.

Thermal Energy Transport

The starting point for this discussion is the statement of the energy transport equation in the form:

$$\nabla \cdot \mathbf{e}_T = \dot{q}''' + \mu \Phi - p \nabla \cdot \mathbf{u} - \frac{\partial \rho e_T}{\partial t} \quad (4)$$

where \mathbf{e}_T is called the energy transport vector and is defined by:

$$\mathbf{e}_T = \rho e_T \mathbf{u} + \dot{\mathbf{q}} \quad (5)$$

Because there is a reference condition for the specific energy, (5) can be replaced by:

$$\mathbf{e}_T = \rho (e_T - e_{ref}) \mathbf{u} + \dot{\mathbf{q}} \quad (6)$$

The form of equation (4) emphasises the fact that the heat source, pressure work, viscous dissipation, heat source and transient terms all contribute to the divergence of the transport vector. Only when the sum of those terms is zero or they can be ignored does the energy transport equation reduce to the solenoidal condition:

$$\nabla \cdot \mathbf{e}_T = 0 \quad (7)$$

General Transport Vector

We can consider \mathbf{e}_T to be an example of a general transport vector which will be denoted here by \mathbf{e} . The general transport equation is,

$$\begin{aligned} \nabla \cdot \mathbf{e} &= \dot{e}''' - \frac{\partial \rho e}{\partial t} \\ &= e_d \end{aligned} \quad (8)$$

where e_d represents the time varying divergence of \mathbf{e} .

Vector and Scalar Potentials for \mathbf{e}

It is useful to consider how the transport vector may be represented by vector and scalar potentials and how these relate to the heat function used for 2D convection.

The Helmholtz decomposition of \mathbf{e} leads to:

$$\mathbf{e} = \nabla \times \Psi_e + \nabla \phi_e \quad (9)$$

The function ϕ_e is a scalar potential for \mathbf{e} and defines its divergence, i.e.:

$$\nabla^2 \phi_e = e_d \quad (10)$$

The vector function Ψ_e is a vector potential for \mathbf{e} . It can be chosen such that:

$$\nabla^2 \Psi = -\nabla \times \mathbf{e} \equiv -\zeta_e \quad \text{and} \quad \nabla \cdot \Psi = 0 \quad (11)$$

where ζ_e is the "transport vorticity" vector.

For 2D processes using x and y Cartesian coordinates, the vector potential and vorticity each have only one component which is aligned in the z direction:

$$\Psi_e = \psi_e \hat{\mathbf{k}} \quad \text{and} \quad \zeta_e = \zeta_e \hat{\mathbf{k}} \quad (12)$$

The function ψ_e is equivalent to a 2D stream function and can be generated by solving:

$$\nabla_{xy}^2 \psi_e = -\zeta_e \quad \text{or} \quad \frac{\partial^2 \psi_e}{\partial x^2} + \frac{\partial^2 \psi_e}{\partial y^2} = -\zeta_e \quad (13)$$

with appropriate boundary conditions.

The scalar potential can be generated by solving:

$$\nabla_{xy}^2 \phi_e = e_d \quad (14)$$

The 2D Heat Function

For the case of the steady state transport of thermal energy we can denote the "stream function" by H so that:

$$\frac{\partial^2 H}{\partial x^2} + \frac{\partial^2 H}{\partial y^2} = -\zeta_e \quad (15)$$

From (12)

$$\begin{aligned} \mathbf{e}_e &= e_x \hat{\mathbf{i}} + e_y \hat{\mathbf{j}} = \nabla \times \psi_e \hat{\mathbf{k}} \\ e_x &= \frac{\partial \psi_e}{\partial y} \quad e_y = -\frac{\partial \psi_e}{\partial x} \end{aligned} \quad (16)$$

This leads to:

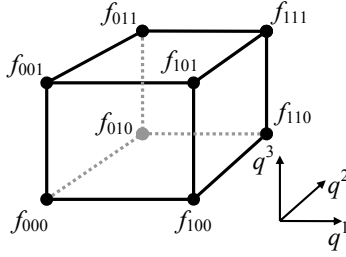


Figure 1 Notation for scalar values stored at the corners of a hexahedral cell. The coordinates have been scaled so that they each have the range $[0,1]$ over the cell.

$$\begin{aligned} \rho u (e_T - e_{ref}) + q_x &= \frac{\partial H}{\partial y} \\ \rho v (e_T - e_{ref}) + q_y &= -\frac{\partial H}{\partial x} \end{aligned} \quad (17)$$

and after using Fourier's law:

$$\begin{aligned} \rho u (e_T - e_{ref}) - k \frac{\partial T}{\partial x} &= \frac{\partial H}{\partial y} \\ \rho v (e_T - e_{ref}) - k \frac{\partial T}{\partial y} &= -\frac{\partial H}{\partial x} \end{aligned} \quad (18)$$

The "thermal vorticity" is:

$$\begin{aligned} \zeta_e &= (\nabla \times \mathbf{e}) \hat{\mathbf{k}} \\ &= (e_T - e_{ref}) \left(\frac{\partial \rho v}{\partial x} - \frac{\partial \rho u}{\partial y} \right) + \rho v \frac{\partial e_T}{\partial x} - \rho u \frac{\partial e_T}{\partial y} \end{aligned} \quad (19)$$

The heat function equation is:

$$\begin{aligned} \frac{\partial^2 H}{\partial x^2} + \frac{\partial^2 H}{\partial y^2} &= -(e_T - e_{ref}) \left(\frac{\partial \rho v}{\partial x} - \frac{\partial \rho u}{\partial y} \right) \\ &\quad - \rho v \frac{\partial e_T}{\partial x} + \rho u \frac{\partial e_T}{\partial y} \end{aligned} \quad (20)$$

Equation (20) can be solved with heat flow boundary conditions (17) to produce H and is identical to the equation used by others [4,24]. It is important to emphasise that this representation can be used only for 2D situations where the transport vector has zero divergence.

The Entropy Transport Vector

Transport vectors for mass, momentum, mechanical energy and entropy can be also defined. A more comprehensive list of examples can be found in [10] and [30]. The transport vector for entropy will be considered here because it always has non-zero divergence and will be used here as an example of a transport process that includes a source.

The entropy transport equation can be written as [10]:

$$\rho \frac{Ds}{Dt} = \frac{\mu \Phi}{T} - \frac{1}{T} \nabla \cdot \mathbf{q} \quad (21)$$

This can be rearranged by differentiating the last term by parts:

$$\frac{\partial \rho s}{\partial t} + \nabla \cdot \rho s \mathbf{u} + \nabla \cdot \left(\frac{\mathbf{q}}{T} \right) = \frac{\mu \Phi}{T} + \nabla \cdot \left(\frac{1}{T} \right) \cdot \mathbf{q} \quad (22)$$

The entropy transport vector is:

$$\mathbf{s} = \rho s \mathbf{u} + \frac{\mathbf{q}}{T} \quad (23)$$

and the transport vector form of the entropy equation is:

$$\nabla \cdot \mathbf{s} = \frac{\mu \Phi}{T} + k \left(\frac{\nabla T}{T} \right)^2 - \frac{\partial \rho s}{\partial t} \quad (24)$$

Particle Tracing

In all situations other than when the transport vector is 2D and divergence free, its visualisation requires the construction of artefacts suitable for the display of vector fields. Vector maps (as in Figure 3) and tangent lines are the most common artefacts used to visualise vector fields. A tangent line to a time varying vector field at the instant t_c can be constructed by numerical approximation to an equation of the form:

$$\mathbf{r}(s) = \mathbf{r}_0 + \int_{s_0}^s \mathbf{e}(\mathbf{r}(\tau), t_c) d\tau \quad (25)$$

It is important that the interpolation procedures used to evaluate \mathbf{e} away from mesh points accurately represent the divergence of \mathbf{e} . For solenoidal fields this condition corresponds to $\nabla \cdot \mathbf{e} = 0$. As discussed in [30], an appropriate strategy is to derive interpolations for the potentials and then differentiate those interpolations to derive the expressions for the velocity. For example, using the notation in Figure 1, the trilinear interpolation for a scalar field ϕ can be represented by:

$$\begin{aligned} \phi &= \left\{ [\varphi_{000}(1-q^1) + \varphi_{100}q^1] \left[(1-q^2) + [\varphi_{010}(1-q^1) + \varphi_{110}q^1] q^2 \right] (1-q^3) \right. \\ &\quad \left. + [\varphi_{001}(1-q^1) + \varphi_{101}q^1] \left[(1-q^2) + [\varphi_{011}(1-q^1) + \varphi_{111}q^1] q^2 \right] q^3 \right\} \end{aligned} \quad (26)$$

For a given mesh cell with its origin at (x_0, y_0, z_0) :

$$q^1 = (x - x_0)/\Delta x \quad q^2 = (y - y_0)/\Delta y \quad q^3 = (z - z_0)/\Delta z \quad (27)$$

and the derivative of ϕ with respect to x is:

$$\frac{\partial \phi}{\partial x} = \frac{1}{\Delta x} \left\{ [\varphi_{100} - \varphi_{000}] \left[(1-q^2) + [\varphi_{110} - \varphi_{010}] q^2 \right] (1-q^3) \right. \\ \left. + [\varphi_{101} - \varphi_{001}] \left[(1-q^2) + [\varphi_{111} + \varphi_{011}] q^2 \right] q^3 \right\} \quad (28)$$

In Cartesian coordinates the expressions for the components of \mathbf{e} becomes:

$$\mathbf{e} = e_x \hat{\mathbf{i}} + e_y \hat{\mathbf{j}} + e_z \hat{\mathbf{k}} \quad \Psi = \psi_x \hat{\mathbf{i}} + \psi_y \hat{\mathbf{j}} + \psi_z \hat{\mathbf{k}} \quad (29)$$

$$\begin{aligned} e_1 &= \frac{\partial \phi}{\partial x} + \frac{\partial \psi_z}{\partial y} - \frac{\partial \psi_y}{\partial z} & e_2 &= \frac{\partial \phi}{\partial y} + \frac{\partial \psi_x}{\partial z} - \frac{\partial \psi_z}{\partial x} \\ e_3 &= \frac{\partial \phi}{\partial z} + \frac{\partial \psi_y}{\partial x} - \frac{\partial \psi_x}{\partial y} \end{aligned} \quad (30)$$

The derivatives appearing in (30) can then be evaluated using approximations of the form (28).

This process has been described very briefly here. As described in [10] it can be readily extended to general curvilinear coordinates.

EXAMPLE PROBLEM

The example of natural convection in a box heated from the side is used here as a basis for a discussion of the issues involved in using transport vector fields for visualisation and for the ways that these concepts might be used for 3D flows.

The cross section of the cavity is square. The vertical wall at $x=0$ is isothermal and hot and the wall at $x=1$ is cold. The other boundaries are adiabatic.

A non dimensional form of the energy equation is:

$$\nabla \theta \mathbf{u} = \nabla^2 \theta \quad (31)$$

Where $T = T_0 + \Delta T \theta$ and the density has been assumed to be constant. The non dimensional energy transport vector is:

$$\mathbf{e}_T = (\theta - \theta_{ref}) \mathbf{u} - \nabla \theta \quad (32)$$

The non dimensional source for the heat vector potential function equation is:

$$\begin{aligned} \nabla \times \mathbf{e}_T &= \nabla \times (\theta - \theta_{ref}) \mathbf{u} \\ &= \nabla \theta \times \mathbf{u} + (\theta - \theta_{ref}) \nabla \times \mathbf{u} \\ &= \nabla \theta \times \mathbf{u} + \theta \zeta - \theta_{ref} \zeta \end{aligned} \quad (33)$$

The isothermal vertical boundaries are represented by $\theta=1$ and $\theta=0$ at $x=0$ and 1 respectively. At $y=0$ and $y=1$ $\frac{\partial \theta}{\partial y} = 0$. For the 3D version of this problem the z boundaries are also adiabatic.

Numerical Procedure

The problem was solved using a vector potential – vorticity method using a collocated grid and central differences for convection. The 2D numerical solutions used a 65 by 65 mesh. 3D problems used a 41 by 41 by 41 mesh. At these resolutions the solutions are known to be good representations of the flow but are not necessarily of benchmark quality which is not essential for the purpose of a discussion of visualization strategies.

The original discussion of the heat function in [4] presented example heatlines for natural convection in a box heated from the side for $Ra = 1.4 \times 10^5$ and $Pr = 7$. These parameters are used here unless specified otherwise.

GENERALISED TREATMENT OF POTENTIALS

The discussions in the previous Section lead to the requirement to generate new representations of heatlines using appropriate vector and scalar potentials. These techniques are illustrated here for the example problem.

The Energy Transport Vector and its Reference Value

Before discussing the use of potentials to generate the heat flux vector it is worth making the observation from (6) that the thermal transport vector can be represented by:

$$\mathbf{e}_T = \rho e_T \mathbf{u} + \dot{\mathbf{q}} - e_{T,ref} \rho \mathbf{u} \quad (34)$$

This means that the thermal transport vector can be expressed in the form:

$$\mathbf{e}_T = \mathbf{e}'_T - \mathbf{e}_{T,ref} \quad (35)$$

$$\mathbf{e}'_T = \rho e_T \mathbf{u} + \dot{\mathbf{q}} \quad \text{and} \quad \mathbf{e}'_{T,ref} = e_{T,ref} \rho \mathbf{u} \quad (36)$$

This is an important observation, because it means that the transport vector can be regarded as being composed of a term which is independent of the reference energy and another term that is the product of the reference energy and the flow mass flux vector. In other words if \mathbf{e}'_T is known, \mathbf{e}_T for a given reference condition can be obtained by simply subtracting a field that is the product of the mass flux vector and the reference specific energy. It follows that vector and scalar potentials can be used to generate \mathbf{e}'_T rather than \mathbf{e}_T .

In terms of a vector potential the energy transport vector is given by:

$$\mathbf{e}'_T = \nabla \times \Psi_e + \nabla \varphi_e \quad (37)$$

The scalar potential satisfies:

$$\nabla^2 \varphi_e = 0 \quad (38)$$

The vector potential satisfies:

$$\nabla^2 \Psi_e = -\zeta_e \quad (39)$$

where:

$$\begin{aligned} \zeta_e &= \nabla \times \mathbf{e}'_T = \nabla \times (\rho \mathbf{u} e_T + \dot{\mathbf{q}}) \\ &= \nabla e_T \times \rho \mathbf{u} + e_T \nabla \times (\rho \mathbf{u}) + \nabla \times \dot{\mathbf{q}} \\ &= \nabla e_T \times \rho \mathbf{u} + e_T \zeta_m + \nabla \times \dot{\mathbf{q}} \end{aligned} \quad (40)$$

and ζ_m is the mass vorticity, $\nabla \times \rho \mathbf{u}$ [10].

If the thermal conductivity is constant, then:

$$\zeta_e = \nabla e_T \times \rho \mathbf{u} + e_T \zeta_m \quad (41)$$

and if the density is constant, equation (41) becomes

$$\zeta_e = \rho \nabla e_T \times \mathbf{u} + \rho e_T \zeta \quad (42)$$

where ζ is the vorticity $\nabla \times \mathbf{u}$.

For the example problem the scalar and vector potential equations are:

$$\nabla^2 \varphi_e = 0 \quad (43)$$

and:

$$\nabla^2 \Psi_e = -\nabla \theta \times \mathbf{u} - \theta \zeta \quad (44)$$

Boundary Conditions for the Energy Transport Vector Potential Equations

For 2D situations, the heat function equation (20) corresponds to using just the vector potential. Although, this can be extended to 3D, [10], the process is complex and involves using auxiliary vector potentials [31] that represent the heat flux passing through boundaries.

An alternative approach is to use the scalar potential to specify the heat flux through the boundaries. The boundary conditions for the vector potential then become the same as those for the fluid motion.

The boundary conditions for φ_e are derived from:

$$\nabla \varphi_s \cdot \hat{\mathbf{n}} = -k \nabla T \cdot \hat{\mathbf{n}} \quad (45)$$

or in terms of the nondimensional variables used in the example problem:

$$\nabla \varphi_s \cdot \hat{\mathbf{n}} = -\nabla \theta \cdot \hat{\mathbf{n}} \quad (46)$$

For the example problem, all boundaries are impermeable and stationary. The boundary conditions for the vector potential are derived from:

$$\Psi_s \cdot \hat{\mathbf{n}} = 0 \quad \nabla \Psi_s = 0 \quad (47)$$

For example for a plane boundary at $x = 0$:

$$\frac{\partial \Psi_s}{\partial x} = 0 \quad \Psi_s = 0 \quad \Psi_z = 0 \quad (48)$$

Entropy Lines

Following the convention used for the energy transport vector, the entropy transport vector can be represented as:

$$\mathbf{s} = \mathbf{s}' - \mathbf{s}_{ref} \quad : \quad \mathbf{s}' = \rho s \mathbf{u} + \frac{\mathbf{q}}{T} \quad \mathbf{s}_{ref} = \rho s_{ref} \mathbf{u} \quad (49)$$

For incompressible flow an equation of state can be used, e.g. (38) in [32], to define s :

$$s - s_{ref} = c_p \ln \frac{T}{T_{ref}} \quad (50)$$

where

$$s = c_p \ln T \quad s_{ref} = c_p \ln T_{ref} \quad (51)$$

In terms of the non dimensional variables used in the example problem and using $\varepsilon = \Delta T / T_{ref}$:

$$\mathbf{s}' = \ln(1 + \varepsilon \theta) \mathbf{u} - \frac{\varepsilon \nabla \theta}{1 + \varepsilon \theta} \quad \mathbf{s}_{ref} = \ln(1 + \varepsilon \theta_{ref}) \quad (52)$$

and the entropy transport equation can be written in the form:

$$\nabla \cdot \mathbf{s}' = \varepsilon^2 \left(\frac{\nabla \theta}{1 + \varepsilon \theta} \right)^2 \quad (53)$$

The equation governing the scalar potential is:

$$\nabla^2 \varphi_s = \varepsilon^2 \left(\frac{\nabla \theta}{1 + \varepsilon \theta} \right)^2 \quad (54)$$

The boundary conditions for φ_s are derived from:

$$\nabla \varphi_s \cdot \hat{\mathbf{n}} = \frac{\mathbf{q} \cdot \hat{\mathbf{n}}}{T} \quad (55)$$

or in terms of non-dimensional variables:

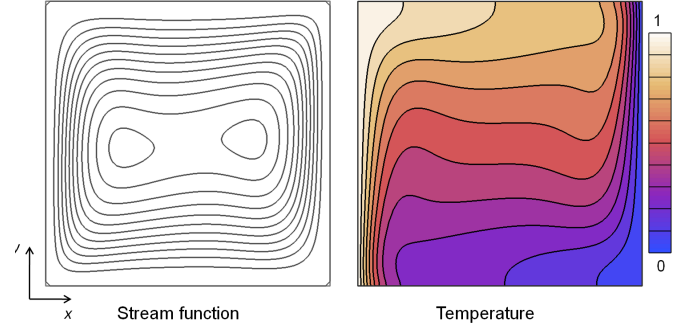


Figure 2 Stream lines and isotherms in a natural convection flow for $Ra=140,000$ and $Pr=7$. On the left vertical wall $\theta=1$ and on the right $\theta=0$. The horizontal boundaries are adiabatic.

$$\nabla \varphi_s \cdot \hat{\mathbf{n}} = \frac{-\nabla \theta}{(1 + \varepsilon \theta)} \quad (56)$$

The vector potential equation is:

$$\nabla^2 \Psi_s = -\nabla \times \mathbf{s}' \quad (57)$$

The boundary conditions for Ψ_s are the same as those for the velocity vector potential.

SAMPLE 2D HEAT FUNCTION VISUALISATIONS AND THE QUESTION OF THE CHOICE OF θ_{ref}

Observations when $\theta_{ref}=0$

It is useful to commence this discussion with examples of conventional heat function representations which use $\theta_{ref} = 0$. The flow stream lines and isotherms for the example problem are shown in Figure 2. These maps are very similar to the maps in [4] and describe the flow and temperature fields which are typical of natural convection in a square cross sectioned cavity.

Heatlines, or iso-lines of the heat function, and heat vectors constructed using $\theta_{ref} = 0$ are shown in Figure 3. The heat function map is very similar to that presented in [4]. The heat function is the normal method of describing heatlines and the underlying vector field has been omitted from most examples in the literature, other than implicitly when 3D or unsteady heatlines have been constructed [10,26,27]. Ironically, despite the 18 years that have elapsed since heatlines were proposed in [4], Hooman [25] appears to be the first to actually publish a heat vector map.

The heat function map in Figure 3 is typical of those that have been presented for closed cavity flows. The heatlines pass from the hot to the cold wall and there is a large region of recirculation that is similar, but not identical, to the fluid motion. Notably the recirculation is asymmetrical and the thermal flow is greater up the hot wall than it is down the cold.

The last observation is not surprising since the thermal convection term $(\theta - \theta_{ref}) \mathbf{u}$ with $\theta_{ref} = 0$ is zero on the cold wall and equal to \mathbf{u} on the hot. The asymmetry is also quite noticeable in the vector map in Figure 3 and there is a region in the bottom right hand corner of the cavity in which the convection is very nearly zero.

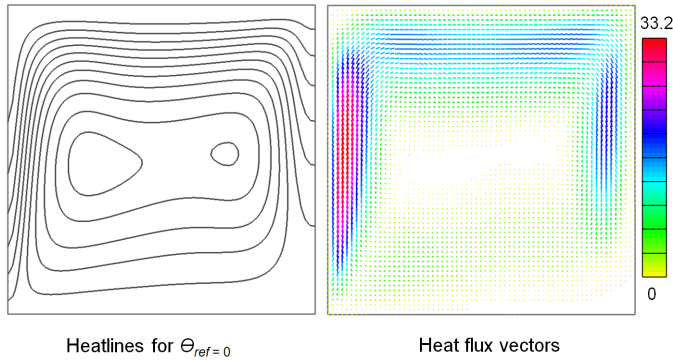


Figure 3 Heatlines and vector map using $\theta_{ref}=0$ for $Ra=140,000$ and $Pr = 7$.

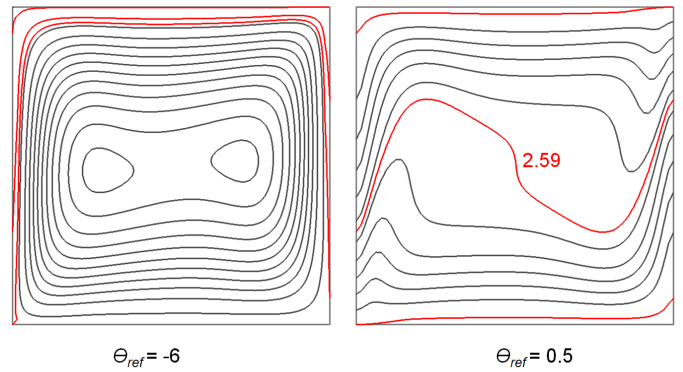


Figure 5 Heatlines for $\theta_{ref} = -6$ and $\theta_{ref} = 0.5$ for $Ra=140,000$ and $Pr = 7$.

Overall Heat Transfer as Described by the Heat Function

For this flow, and mesh used, the total non dimensional heat flow through the left wall as estimated using a second order one sided approximation for the temperature gradient and trapezoidal integration is 5.24. Because approximation to the gradient is different from the central difference approximation used to set the adiabatic condition there is a net heat flow of 0.06 through each horizontal boundary. The difference between the values of two iso-lines of the heat function is proportional to the heat flow through the region they delineate. In Figure 4(a) the 5.18 iso-line at the top of the box indicates how the hot wall supplies the 0.06 leakage through the top surface. The 0.0 iso-line leaves the bottom of the hot wall, passes around the recirculating core and leaves the cavity a small distance up the cold wall. The -0.06 iso-line leaves the bottom surface very near the cold right hand wall, circulates clockwise around the core and then leaves the cavity near the bottom of the cold wall. The 0.06 heat flow which leaves the bottom surface passes around the core to the lowest section of the cold wall. The heat that is transferred between the two walls follows a path, between the 0.0 and 5.18 heatlines, that passes up the hot wall, across the top of the cavity and down the cold wall.

The Influence of the Value of θ_{ref}

In Figure 4(b) the $H=0$ iso-lines have been constructed for

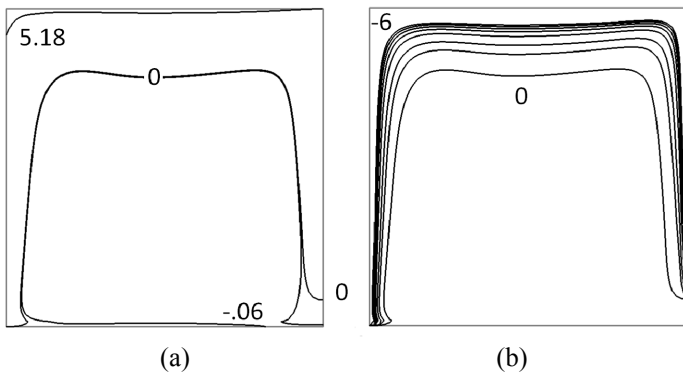


Figure 4 (a) Heatlines for $\theta_{ref}=0$ for $Ra=140,000$ and $Pr=7$. The total non dimensional heat flow is 5.24. The lines shown indicate the limits of the recirculation region. (b) $H=0$ lines for maps with $\theta_{ref} = 0, -0.5, -1, -2, -3, -4, -5$ and -6 .

$\theta_{ref} = 0, -0.5, -1, -2, -3, -4, -5$ and -6 indicate the effect of θ_{ref} on the boundary of the heat flow path. As θ_{ref} becomes increasingly negative its effect on this boundary becomes almost asymptotic.

Negative values of θ_{ref} always ensure that θ is positive everywhere in the flow. θ maps to real temperatures via the definition of ε as $\Delta T/T_{ref}$. For the results in Figure 4, T_0 and ΔT were 300 K and 50 K respectively. For these values, $\theta_{ref} = -6$ corresponds to $T_{ref} = 0$ K.

Although it appears that another set of parameters have been added to the specification of the visualisation, the results in Figure 4(b) suggest that a heatline visualisation may be essentially invariant for $\theta_{ref} \leq -3$.

The heatline visualisation for $\theta_{ref} = -6$ is shown in Figure 5(a). The heatline pattern is very similar to the flow stream function shown in Figure 2. The red lines indicate the boundaries of the heat flow paths and these exhibit the effects of conduction close to the wall.

Positive values of θ_{ref} lead to negative values of θ in the heat transfer field. This leads to the problematic concept of heat travelling from 'cold to hot'. Using $\theta_{ref} = 0.5$ as suggested in [10] produced the visualisation in Figure 5(b) which has no recirculation. This visualisation was suggested because it simplified the structure of the heatline map and possessed the anti-symmetry of the underlying problem. Note that the 2D heatlines have the same entry and exit points for all values of θ_{ref} . Hence although the $\theta_{ref} = 0.5$ lines indicate that the heat flows "backwards" within the cavity the entry and exit points still match the correct heat flow conventions.

RE-EXAMINATION OF THE ROLE OF CONDUCTION IN THE HEAT TRANSFER PROCESS

The role of the heat conduction field as an aid for the visualization of the thermal process is now considered. The conduction lines can be constructed using temperature as a scalar potential for the heat flux, i.e.

$$\dot{\mathbf{q}} = -\nabla\theta \quad (58)$$

Using the principles described by equation (30), this can be built into a magnet line tracing procedure. The results for the example problem are presented in Figure 6.

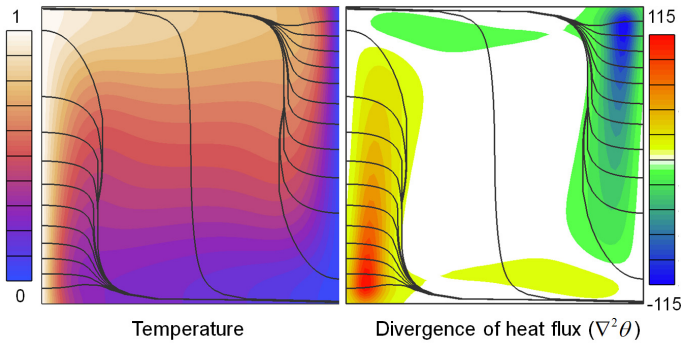


Figure 6 Lines of the heat conduction field superimposed on maps of temperature and the divergence of the heat flux vector, for $Ra=140,000$ and $Pr=7$.

These lines cannot be represented by the iso-lines of a scalar function and must be traced from $\dot{\mathbf{q}}$. The lines in Figure 6 were launched from the boundaries using equal increments of 0.518 in heat flow. The divergence of $\dot{\mathbf{q}}$ is non-zero, because of the effects of convection. The conduction lines appear to indicate that all the heat from the cold wall converges along a single line to proceed to the cold wall. Similarly the distribution of heat leaving the cold wall comes from a single line that starts from the hot wall.

This of course is not really the case. The heat is removed from the "conduction field" and is transferred to the "flow field". This occurs in the regions of high divergence. The conduction heatlines converge along the edges of the regions of high divergence. As the flow recirculates it picks up heat as it passes up the hot wall and releases heat as it passes down the cold. This is the conventional understanding of this process which has been explained here using the temperature and conduction flux lines, rather than using heatlines.

Conduction lines for $Ra=10^4$ and 10^6 in an air filled cavity are presented in Figure 8. The conduction lines have the same general relationship with the regions of high divergence as they do for the flow in Figure 6.

The conduction and flow lines are compared with $\theta_{ref}=0$ heatlines in Figure 9. Note that the conduction lines match with the heatlines at the boundaries.

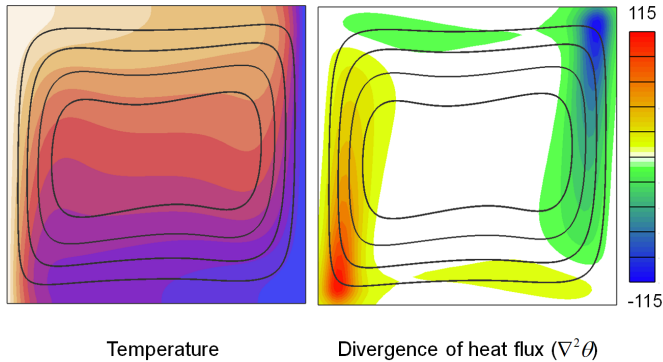


Figure 7 Flow lines superimposed on maps of the temperature and the divergence of the heat flux vector for $Ra=140,000$ and $Pr=7$.

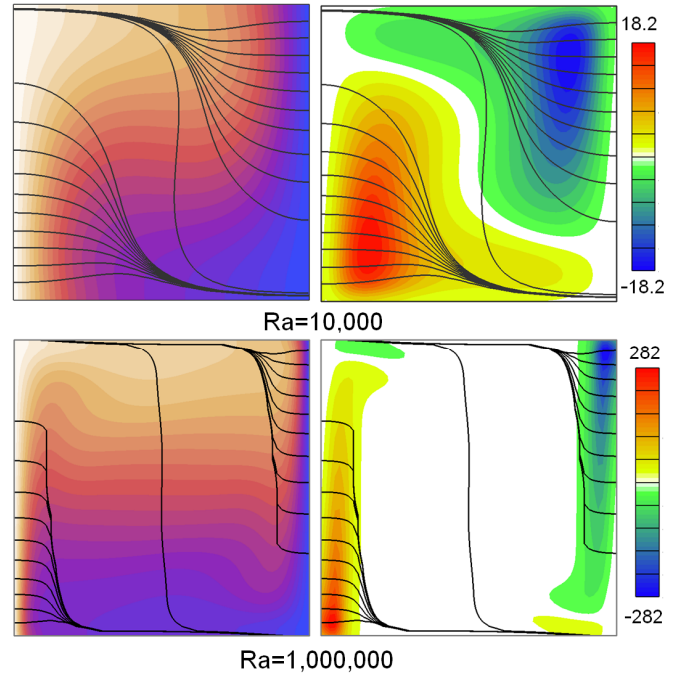


Figure 8 Heat conduction lines for an air filled cavity ($Pr=0.71$). Maps as in Figure 6.

Potentials Used in the Construction of Heatlines

The lines and associated maps described so far have been based on the heat function which was obtained by solving equation (44) with boundary conditions that represented the heat flux conditions applied to the vector potential (or heat function). It is illustrative to now consider how the potentials described by both equations (43) and (44) can be used. These potentials are illustrated in Figure 10 and Figure 11. The scalar potential in the left hand side of Figure 10 is represented as a shaded contour map. The representation on the right hand side contains the iso-lines of that map together with vectors that indicate the direction of heat flow (which for the scalar potential is the direction of $\nabla\phi$). The magnitude of the heat flux is indicated as a colour shaded map.

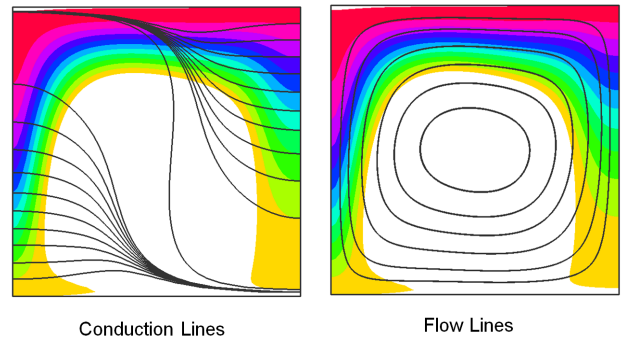


Figure 9 Conduction and flow lines for $Ra=10,000$ and $Pr=0.71$, superimposed on maps of the heat function. The colour contours range from 0 to 5.18. The white region represents the recirculating region of the heatlines.

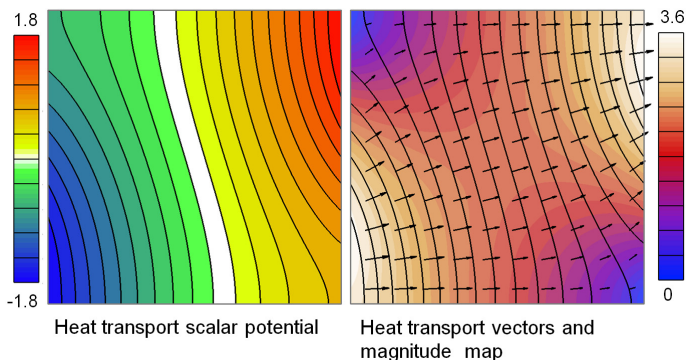


Figure 10 The heat transport scalar potential. The scalar potential is represented by its iso-lines (black). The vectors represent the gradient of the scalar potential. The colour map in the right hand image is the magnitude of the gradient.

The vector potential has been visualized in Figure 11 by drawing iso-lines of its z component. These lines indicate that the effect of the thermal transport vorticity is to induce a recirculating flow.

When the reference temperature is changed, it is only the vector potential for the energy transport vector that changes. The two maps in Figure 11 show the vector potential for $\theta_{ref}=0.5$ and $\theta_{ref}=-5$. For both cases, and indeed for all values of θ_{ref} , the scalar potential is the same as that illustrated in Figure 10. It is that potential that matches the heat flux boundary conditions. The vector potential, on the other hand, determines the effects of the thermal vorticity, which has two contributions (40). The first is the cross product of the gradient of specific energy and the mass flux. This component is independent of the reference conditions for enthalpy.

The second contribution is the product of the specific energy and the mass vorticity. It is this component which is dependent on the assumed reference conditions and it determines the amount of vorticity that is subtracted from the thermal flow to effectively provide a moving frame of reference for thermal transport. For the scaling used for the example problem, the non-dimensional temperature lies in the interval $[0,1]$ and the natural base solution corresponds to $\theta_{ref}=0$. However, the problem could have been scaled so that θ was in the interval $[-0.5,0.5]$ which would produce a natural base solution that corresponded with $\theta_{ref}=0.5$. In any event, the visualisation can be adjusted by subtracting an appropriate "amount" of flow from the "base" visualisation.

The visualisations in Figure 11 were obtained in this way. The vector potential used to produce the maps for $\theta_{ref}=0.5$ is equal to the base thermal vector potential ($\theta_{ref}=0.0$) with 0.5 times the flow vector potential added to it. The result is the two counter rotating flow contributions illustrated in Figure 11. When these are combined with the scalar potentials through flow contribution, the result is the heatlines shown in colour. These heatlines have no recirculation.

The visualisation for $\theta_{ref}=-5$ were obtained by subtracting 5.5 times the flow vector potential from the one with $\theta_{ref}=0.5$.

Note that the heatlines presented in Figure 9 and Figure 11 are maps of the heat function obtained using the conventional

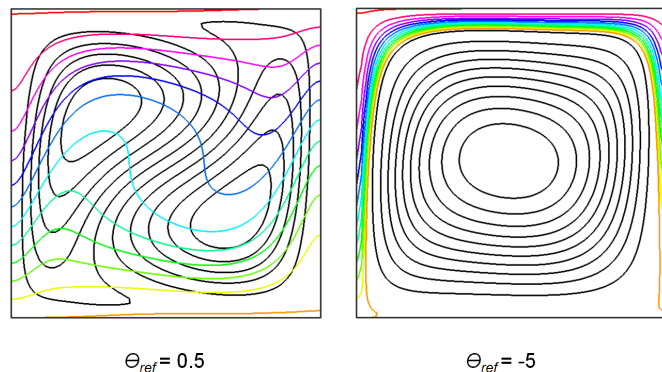


Figure 11 Maps of the z component of the vector potential for $Ra=10,000$ and $Pr=0.71$ for $\theta_{ref}=0.5$ and $\theta_{ref}=-5$.

method. The lines can also be traced using the scalar and vector potentials. Results using this process were identical to the lines presented in these Figures.

ENTROPY TRANSPORT

The transport of entropy in the same cavity is now considered. For this study $Ra=10,000$ and $Pr=0.71$. The temperature difference, ΔT , was set to 200 K and T_{ref} to 300 K. These values were chosen to produce large numerical values of entropy generation so that its transport could be more easily visualized, the purpose being to understand how the entropy source contributes to the transport process.

The rate at which entropy leaves the cavity through the cold wall is greater than the rate it enters through the hot wall. For this problem the nondimensional entropy flow through the hot wall is 0.89, the flow through the cold wall is 1.49 and the total volumetric production is 0.6. Following [33] the total entropy production leads to an estimated Nusselt number of 2.235, compared with 2.242 calculated directly from the temperature field.

Because the entropy transport vector defined by (49) is not solenoidal, it must be represented by both the scalar and vector potentials. The potential is found by solving the Poisson equation (43), with the entropy flow rates applied on the boundaries using (56). The resulting solution and the associated vector field are shown in Figure 12 along with the entropy source. As expected the entropy source is strong near the walls and it is considerably stronger near the cold wall than it is near the hot wall. The scalar potential confirms that the heat transfer through the cold wall is greater than it is through the hot wall. (Compare the visualisation of the scalar potential in Figure 12 with that in Figure 10 for which the heat flows through both walls are identical.)

The vector potential for $\theta_{ref}=0$ is illustrated in Figure 13. It closely resembles the vector potential for energy transport. The boundary conditions for this potential correspond to those for the flow vector potential. The result of combining the two potentials to produce the entropy transport vector is illustrated in the right hand diagram in Figure 13. These lines must be constructed using a tracing procedure. They cannot be

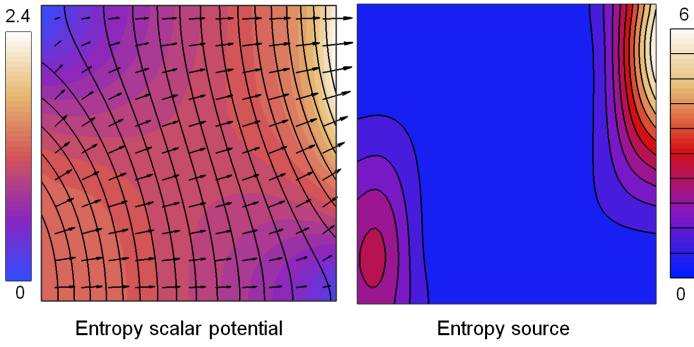


Figure 12 Scalar potential for entropy and the entropy source. The scalar potential is represented by its iso-lines (black). The vectors represent the gradient of the scalar potential. The magnitude of the gradient is displayed as a colour map.

constructed as contours of any combination of the scalar potential and components of the vector potential. The lines correspond with those represented by the map in the background of Figure 9. However, the circulating entropy lines in the central region of the cavity spiral, whereas the heatlines don't. For this version of the entropy line visualisation (corresponding to $\theta_{ref}=0$), the spiralling flow provides a route for the entropy generated within the cavity to progress to the cold wall.

This entropy flow illustrated in Figure 13 raises the question of how the flow of entropy generated within the cavity is affected by changes in θ_{ref} . For $\theta_{ref}=0.5$, there is no recirculating region. The generated entropy contributes to the entropy flow by increasing the strength of the entropy flux, in much the same way that the entropy flux predicted by the scalar potential increases near the cold wall. When there is circulation of the entropy lines, some of the generated entropy is carried by a spiralling flow. The lines in the right hand image in Figure 14 are the lines that delineate the recirculating region for different values of θ_{ref} . As θ_{ref} decreases, this boundary moves higher up the cold wall.

Bearing in mind that the region above this boundary carries all the entropy that enters the hot wall, this observation means

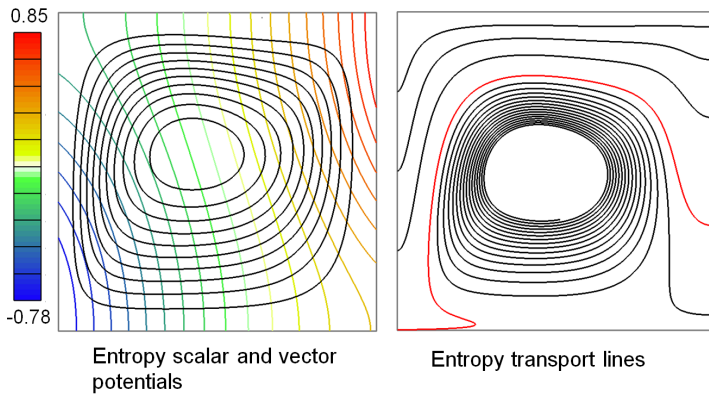


Figure 13 Entropy scalar and vector potentials for $Ra=10,000$ and $Pr=0.71$. The transport lines have been traced using a vector and scalar potential tracing procedure.

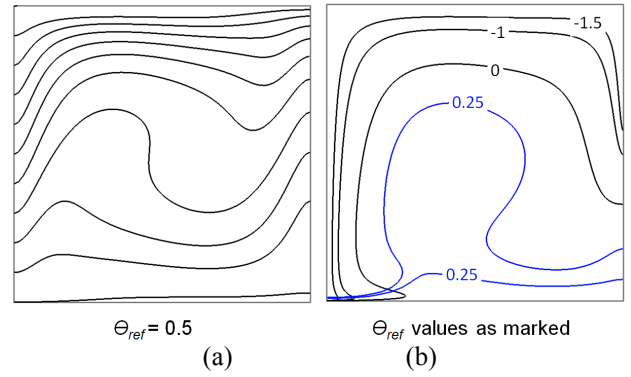


Figure 14 (a) Entropy transport lines for $\theta_{ref}=0.5$. (b) Limiting transport lines for several values of θ_{ref} . The two blue lines for $\theta_{ref}=0.25$ are necessary because some of the entropy from the bottom of the hot wall passes below the region of circulation.

that the assumed reference condition for the visualisation influences the interpretation of how entropy generated within the cavity is combined with the entropy that is passing through it. The reference condition has appeared to influence the mechanism of entropy transport. This does raise a serious question about the validity of the transport vector approach as a visualization strategy.

3D RESULTS

For heat transfer problems that are not 2D and steady, the heatlines must be constructed by integration of the equations defining tangents to the transport vector and has been the approach that has been already used to extend the heatline approach [10,26-28]. These integrations must be executed carefully using interpolation schemes that accurately represent the underlying properties, of the transport vectors. As suggested in [10] an appropriate strategy is to derive appropriate potentials from the energy transport vector and use them to construct the interpolation formulae. In [10] a vector potential was used to generate mass conservative interpolations.

Although the fluid motion is closed within the cavity, the energy flux vector represents a through flow of energy and the boundary conditions for Ψ_e are that its curl must represent this flow through a boundary. In [10] the boundary conditions for Ψ_e were set by using the auxiliary potential proposed in [31]. This is a fairly complex process and involves solving a 2D Poisson equation on every boundary through which there is a heat flow.

Alternatively a scalar potential can be used to accommodate the heat flow boundary conditions in the same way that has been demonstrated for 2D problems. The vector potential then has the same boundary conditions as those for the fluid motion, (e.g. for closed flows (47)). This is a much simpler process and the boundary conditions for the scalar potential can be derived in a straight forward manner using (45). This has now been implemented and the 3D visualisations use this approach.

There is no simple whole field approach for the visualisation of the energy transport vector. A set of heat flow

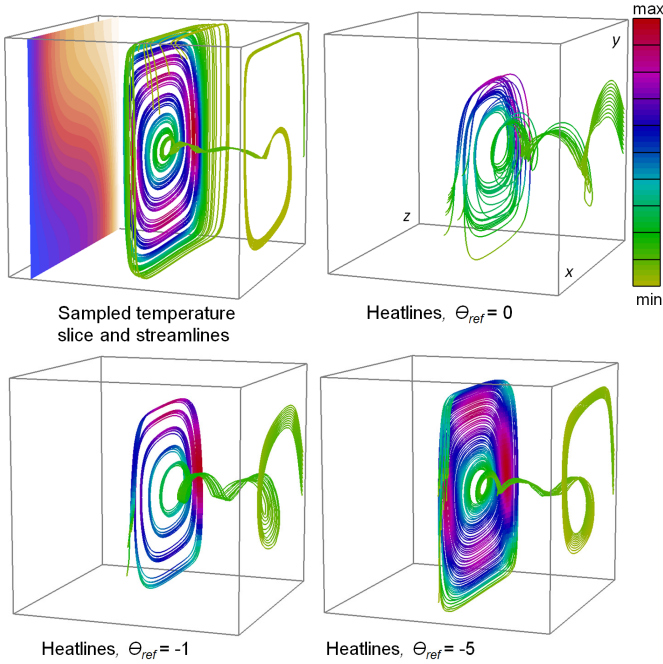


Figure 15 3D results for $Ra=10,000$ and $Pr=0.71$ natural convection in a cube. The rear wall is hot.

paths for different values of θ_{ref} are presented in Figure 15. These have been released from a line near the mid height of the hot wall and in the corner edge near an end wall. Heat from this region passes to the central symmetry plane before exiting via the cold wall. Heatlines released on a line along the hot wall in Figure 16 show that as θ_{ref} becomes more negative, the region of recirculation grows in the same way that it does in 2D.

In the 2D maps, the mapping between entry and exit points for the heatlines is not affected by the value of θ_{ref} . From our results this seems unlikely for 3D flows. However, despite the care with which our line tracing algorithms have been constructed this observation is not easily supported nor contradicted.

ENTROPY LINES

Preliminary entropy lines for the example problem with $Ra=10,000$ and $Pr=0.71$, $\Delta T=200$ K and $T_0=300$ K are presented. These are the same conditions as for the 2D simulations. For the chosen values of ΔT and T_0 , 0 K corresponds to $\theta=-1.5$.

Heatlines and entropy lines are compared in Figure 17. The lines were traced in reverse so that they indicate where the transferred property arriving at the line of release came from. This shows the same general trend as the heatlines in Figure 15, that heat (and entropy) exiting near the cavity central symmetry plane comes from the hot wall close to the adiabatic end walls. The essential result from the comparison shown in Figure 17 is that there appears to be very little difference between the heatlines and the entropy lines. Most of the exploratory line tracing that we have conducted has supported this observation. The spiralling flows which are part of the fluid motion appear

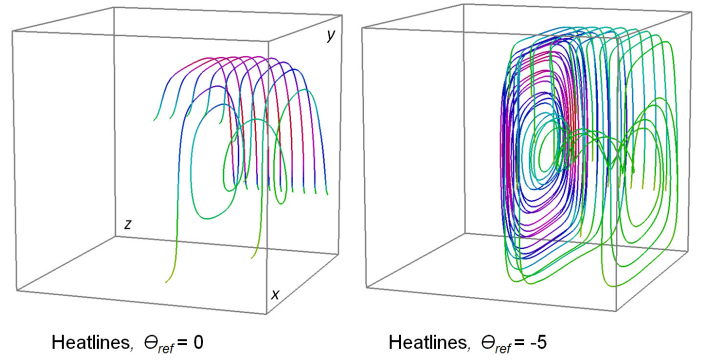


Figure 16 Heatlines from 9 points evenly distributed on the line joining $(1,0.25,0.05)$ and $(1,0.25,0.45)$, for two values of θ_{ref} . The hot wall is at the rear of this view.

to be the primary mechanism for removing entropy generated in the cavity.

The results that do show a measurable difference between heatlines and entropy lines are those for $\theta_{ref}=0.5$. Trajectories released on a horizontal line at $y=0.25$ are shown in Figure 18. These indicate that away from the end walls and the central symmetry plane, entropy lines ascend more quickly than do the heatlines. This occurs in 2D as well. The visualisation that has no recirculation has indicated a measurable difference between the heatline and entropy lines, resulting from the entropy source.

CONCLUSIONS

It has been shown that vector and scalar potentials have roles in creating visualisation artefacts for transport vectors. The original motivation was to use these potentials to create interpolation procedures that accurately represented vector fields having zero divergence. However splitting the transport vectors into curl and divergence free contributions has led to an understanding of how techniques such as the heatline approach might be properly extended to problems involving generation processes.

For the energy transport vector, a combined scalar and vector potential method for constructing the energy transport lines has been created. By assigning the energy flow boundary

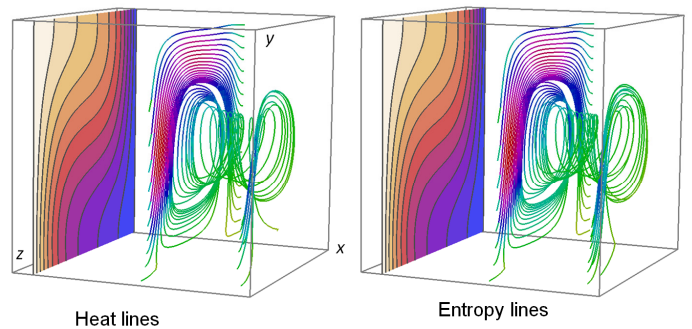


Figure 17 Heatlines and entropy lines in a cavity with $Ra=10,000$ and $Pr=0.71$ for $\theta_{ref}=0$. The front wall is hot.

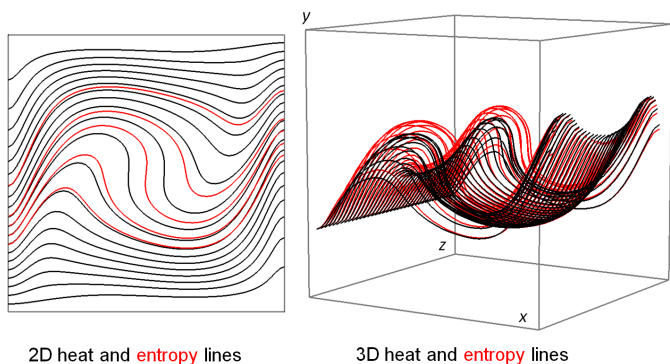


Figure 18 Entropy lines for convection when $Ra=10,000$ and $Pr=0.71$, using $\theta_{ref}=0.5$. In the 3D model the lines have been released on a horizontal line located at $z=0.25$ up the hot wall.

conditions to the scalar potential, the vector potential is then very similar to the flow vector potential. For the closed cavity problems considered here, the vector potential represents recirculations induced by "thermal vorticity".

The decomposition used in deriving the combined scalar and vector potential approach lead to the realisation that the effects of the assumed reference conditions can be represented by a term that is equivalent to the product of the flow field and that reference condition. Having obtained a transport vector field or its scalar and vector potential representations for a particular reference condition, other representations can be easily generated by adding or subtracting an appropriate amount of "flow".

The last comment leads to the question of what constitutes an appropriate "base" solution. The scaling used in this research has used the conventional approach of assigning the reference condition to the coldest point in the domain. Mathematically a "cleaner" base solution is that where the reference condition negates all recirculation. From a physical point of view, a condition that represents absolute zero temperature, or is sufficiently below the temperature range of the phenomenon being studied that a transport line visualisation is essentially invariant, may be another acceptable reference condition.

The entropy transport vector for a non trivial situation has a non zero divergence. In this case the use of a scalar potential is essential to properly handle the entropy flow – internal generation balance. In this case the assumed reference condition influences the way that entropy generated within a cavity combines with the entropy passing through it. There is no reason to assume that this is an issue for just entropy transport; it is likely to be an issue for the transport of any quantity for which there is a volumetric source or sink. This observation increases the importance of the need to resolve the "reference condition" issue.

Results for 3D are similar to those for 2D, insofar as visualisations using tangent lines are concerned. In 3D it is much more difficult to determine how the internally generated entropy contributes to the overall process.

As part of this investigation, the conduction heatlines were constructed from the convection temperature field. This vector

field has non zero divergence that couples it to the heat carrying capacity of the moving fluid. The combination of conduction field lines, the divergence maps and the flow lines may eventually prove to be more useful than visualisations based on the transport vectors.

REFERENCES

- [1] Harlow, F. H., Shannon, J. P. and Welch, J. E., 1965, Liquid Waves by Computer, *Science*, Vol. 149, No. 3688, pp 1092-1093.
- [2] Harlow, F. H. and Shannon, J. P., 1967, Distortion of a Splashing Liquid Drop, *Science*, Vol. 157, No. 3788, pp 547-550.
- [3] Fromm, J., 1964, The Time Dependent Flow of an Incompressible Fluid, *Methods of Computational Physics*, Vol. 3, pp 345-382.
- [4] Kimura, S. and Bejan, A., 1983, The "Heatline" Visualization of Convective Heat Transfer, *ASME Journal of Heat Transfer*, Vol. 105, pp 916-919.
- [5] Holst, P. H. 1970 A Theoretical and Experimental Investigation of Natural Convection in a Porous Medium, Calgary, University of Calgary.
- [6] Holst, P. H. and Aziz, K., 1972, Transient Three Dimensional Natural Convection in Confined Porous Media, *International Journal of Heat and Mass Transfer*, Vol. 15, No. 1, pp 73-90.
- [7] Mallinson, G. D. and de Vahl Davis, G., 1973, The Method of the False Transient for the Solution of Coupled Elliptic Equations, *Journal of Computational Physics*, Vol. 12, No. 4, pp 435-461.
- [8] Mallinson, G. D. and de Vahl Davis, G., 1977, Three Dimensional Natural Convection in a Box: A Numerical Study, *Journal of Fluid Mechanics*, Vol. 83, No. 1, pp 1-31.
- [9] Buning, P. G., 1987, Sources of Error in the Graphical Analysis of CFD Results, *Journal of Scientific Computing*, Vol. 3, No. 2, pp 149-164.
- [10] Mallinson, G. D., 2009, Vector Lines and Potentials for Computational Heat Transfer Visualisation, *International Journal of Heat and Mass Transfer*, Vol. 52, pp 4008-4020.
- [11] Greywall, M. S., 1988, Streamwise Computation of Three-Dimensional Incompressible Potential Flows, *Journal of Computational Physics*, Vol. 78, pp 178-193.
- [12] Greywall, M. S., 1993, Streamwise Computation of Three-Dimensional Flows Using Two Stream Functions, *Journal of Fluids Engineering*, Vol. 115, pp 233-238.
- [13] Keller, J. J., 1996, A Pair of Stream Functions for Three-Dimensional Vortex Flows, *Z Agnew Math Phys*, Vol. 47, pp 821-836.
- [14] Beale, S. B., 1993, A Numerical Scheme for the Generation of Streamlines in Three Dimensions, *CFD93, Conference of the CFD Society of Canada*, Montreal.
- [15] Beale, S. B., 1997, Visualisation of Three-Dimensional Flow Fields Using Two Stream Functions, *10th International Symposium on Transport Phenomena*, Kyoto, Japan.
- [16] Kenwright, D. and Mallinson, G., 1993, A 3-D Streamline Tracking Algorithm Using Dual Stream Functions, *IEEE Visualization '93*, Boston.
- [17] Knight, D. and Mallinson, G., 1996, Visualising Unstructured Flow Data Using Dual Stream Functions, *IEEE Transactions on Visualization and Computer Graphics*, Vol. 2, No. 4, pp 355-363.
- [18] Li, Z. and Mallinson, G. D., 2002, Dual Stream Functions for Linearly Varying Momentum Vector Fields over Tetrahedral Domains, *10th International Symposium on Flow Visualization*, Kyoto, Japan.
- [19] Bejan, A., 1984 *Convective Heat Transfer*, John Wiley and Sons, Inc.

- [20] Kaluri, R. S., Basak, T. and Roy, S., 2009, Bejan's Heatlines and Numerical Visualization of Heat Flow and Thermal Mixing in Various Differentially Heated Porous Square Cavities, *Numerical Heat Transfer, Part A: Applications: An International Journal of Computation and Methodology*, Vol. 55, No. 5, pp 487 - 516.
- [21] Deng, Q.-H. and Tang, G.-F., 2002, Numerical Visualization of Mass and Heat Transport for Mixed Convective Heat Transfer by Streamline and Heatline, *International Journal of Heat and Mass Transfer*, Vol. 45, pp 2387-2396.
- [22] Costa, V. A. F., 2003, Unified Streamline, Heatline and Massline Methods for the Visualization of Two-Dimensional Heat and Mass Transfer in Anisotropic Media, *International Journal of Heat and Mass Transfer*, Vol. 46, No. 8, pp 1309-1320.
- [23] Mukhopadhyay, A., Qin, X., Aggarwal, S. K. and Puri, I. K., 2002, On Extension of "Heatline" and "Massline" Concepts to Reacting Flows through Use of Conserved Scalars, *Journal of Heat Transfer*, Vol. 124, No. 4, pp 791-799.
- [24] Bejan, A., 2004 *Convection Heat Transfer*, John Wiley and Sons, Inc.
- [25] Hooman, F., 2010, Energy Flux Vectors as a New Tool for Convection Visualization, *International Journal of Numerical Methods for Heat and Fluid Flow*, Vol. 20, No. 2, pp 240-249.
- [26] Mahmud, S. and Fraser, R. A., 2007, Visualizing Energy Flows through Energy Streamlines and Pathlines, *International Journal of Heat and Mass Transfer*, Vol. 50, No. 19-20, pp 3990-4002.
- [27] Speetjens, M. F. M. and van Steenhoven, A. A., 2010, Visualisation of Heat Transfer in 3D Unsteady Flows, *International Journal of Thermal Sciences*, Vol. 49, No. 7, pp 1103-1114.
- [28] Speetjens, M. F. M. and van Steenhoven, A. A., 2011, Visualization of Heat Transfer in Unsteady Laminar Flows, *Computational Thermal Sciences*, Vol. 3, No. 1, pp 31-47.
- [29] Costa, V. A. F., 1999, Unification of the Streamline, Heatline and Massline Methods for the Visualization of Two-Dimensional Transport Phenomena, *International Journal of Heat and Mass Transfer*, Vol. 42, No. 1, pp 27-33.
- [30] Mallinson, G. D. and Norris, S. E., 2010, Fundamentals of Computational Fluid Dynamics, in *Mathematical Modeling of Food Processing*, Farid, M. (Ed.), Boca Raton, Florida, CRC Press / Taylor & Francis Group.
- [31] Hirasaki, G. J. and Hellums, J. D., 1968, A General Formulation of the Boundary Conditions on the Vector Potential in Three-Dimensional Hydrodynamics, *Quarterly of Applied Mathematics*, Vol. 26, pp 331-342.
- [32] Weigand, B. and Birkefeld, A., 2009, Similarity Solutions of the Entropy Transport Equation, *International Journal of Thermal Sciences*, Vol. 48, No. 10, pp 1863-1869.
- [33] Norris, S. E. and Mallinson, G. D., 2007, Volumetric Methods for Evaluating Energy Loss and Heat Transfer in Cavity Flows, *International Journal for Numerical Methods in Fluids*, Vol. 54, No. 12, pp 1407-1423.